PHYSOR 2014 - The Role of Reactor Physics toward a Sustainable Future
The Westin Miyako, Kyoto, Japan, September 28 - October 3, 2014, on CD-ROM (2014)

POLARIS: A NEW TWO-DIMENSIONAL LATTICE PHYSICS ANALYSIS CAPABILITY FOR THE SCALE CODE SYSTEM

Matthew A. Jessee, William A. Wieselquist, Thomas M. Evans, Steven P. Hamilton, Joshua J. Jarrell, Kang Seog Kim, Jordan P. Lefebvre, Robert A. Lefebvre, Ugur Mertyurek, Adam B. Thompson, Mark L. Williams
Oak Ridge National Laboratory, P. O. Box 2008, Oak Ridge, TN 37831 USA
jesseema@ornl.gov,wieselquiswa@ornl.gov

ABSTRACT

Polaris is a new 2-dimensional (2-D) lattice physics capability in the SCALE code system for the analysis of light water reactor fuel designs. In this paper, the Polaris calculation methods are summarized and results are provided for a series of computational benchmarks. The summary includes the implementation of the relatively new resonance self-shielding approach called the embedded self-shielding method, the implementation of a new 2-D method-of-characteristics neutron transport solver, and the integration of the SCALE/ORIGEN depletion and decay solver for depleting material compositions. Polaris calculations are compared with reference continuous energy Monte Carlo solutions for a UO_2 fuel computational benchmark. Because Polaris is integrated into the SCALE code system, Polaris has been utilized as part of the new SCALE/Sampler code sequence, which provides uncertainty analysis for the impact of cross-section uncertainties on lattice physics calculations. SCALE/Sampler results are summarized for selected benchmark calculations.

Key Words: **lattice physics, cross-section uncertainty analysis**

1. INTRODUCTION

Polaris is a new 2-dimensional (2-D) lattice physics analysis capability within the SCALE code system [1] for the modeling and simulation of light water reactor (LWR) fuel designs. Polaris was developed as an alternative to the current lattice physics capability in SCALE provided by the TRITON control module. Released in 2004 as part of SCALE 5.0, TRITON is a general purpose control module that provides a wide range of analysis capabilities, including lattice physics. The key computational features of TRITON include pointwise unit-cell–based self-shielding with CENTRM, user-defined general-geometry multigroup transport using 2-D S_N or 3-D Monte Carlo methods, depletion calculations via the ORIGEN depletion solver, and automation of adjoint transport calculations for sensitivity and uncertainty analysis of 2-D models. Although this set of features provide modeling flexibility, the TRITON input requirements and calculation run times limit its application for production-level lattice physics analysis. Therefore the Polaris initiative is to provide a new LWR lattice physics capability in SCALE with an easy-to-use input format and faster run-times.

In Section 2, the Polaris calculation methods and implementation are summarized. Section 2 expands on the implementation of a new self-shielding method called the embedded self-shielding

method (ESSM) [2], as well as other calculation methods. The application of Polaris for several computation benchmarks is provided in Section 3. Section 3 also demonstrates the application of Polaris for the propagation of cross-section uncertainties through lattice physics calculations. The uncertainty quantification for lattice physics parameters is performed by Polaris calculations as part of the new SCALE/Sampler sequence [3]. Both Polaris and Sampler will be released with SCALE 6.2 in 2014.

2. METHODS

2.1. ESSM Implementation

ESSM has been implemented into Polaris for calculating self-shielded multigroup cross sections. Similar to the subgroup method, ESSM performs a series of fixed source transport calculations to determine the background cross section used in equivalence-theory–based cross-section interpolation. Although ESSM is described in detail in Ref. [2], a brief summary of the method and its implementation into Polaris is presented in this section.

ESSM employs the intermediate resonance (IR) approximation to the continuous energy (CE) slowing down equation. Using the IR approximation, the CE slowing down equation within energy group g can be written as follows:

$$\hat{\Omega}\cdot\nabla\psi_g(\bar{r},E,\hat{\Omega})+\Sigma_{t,g}(\bar{r},E)\psi_g(\bar{r},E,\hat{\Omega})=\frac{1}{4\pi}\Sigma_{wr,g}(\bar{r})\phi_g(\bar{r},E)+\frac{1}{4\pi}\frac{\Sigma_{nr,g}(\bar{r})}{E} \tag{1}$$

where

$$\begin{aligned}\Sigma_{wr,g}(\bar{r}) &\equiv \sum_i N_i(\bar{r})(1-\lambda_{g,i})\sigma_{p,i},\\ \Sigma_{nr,g}(\bar{r}) &\equiv \sum_i N_i(\bar{r})\lambda_{g,i}\sigma_{p,i}, \text{ and}\\ \Sigma_{t,g}(\bar{r},E) &\equiv \sum_i N_i(\bar{r})(\sigma_{a,i}(E)+\sigma_{p,i})\\ &= \Sigma_{wr,g}(\bar{r})+\Sigma_{nr,g}(\bar{r})+\sum_i N_i(\bar{r})\sigma_{a,i}(E)\end{aligned}$$

In Eq. (1), $\psi_g(\bar{r},E,\hat{\Omega})$ and $\phi_g(\bar{r},E)$ are the angular flux and scalar flux, respectively. $\lambda_{g,i}$ and $\sigma_{p,i}$ are the IR parameter and potential scattering cross section for nuclide i. In the current Polaris implementation, the nuclide-wise CE absorption cross section $\sigma_{a,i}(E)$ accounts only for (n,γ) and (n,f) contributions. The material-wise cross sections $\Sigma_{wr,g}(\bar{r})$ and $\Sigma_{nr,g}(\bar{r})$ are the wide-resonance and

narrow-resonance macroscopic potential scattering cross sections for energy group g. Integrating Eq. (1) over the group g energy boundaries produces the following multigroup equation:

$$\hat{\Omega}\cdot\nabla\psi_g(\bar{r},\hat{\Omega})+\Sigma_{t,g}(\bar{r})\psi_g(\bar{r},\hat{\Omega})=\frac{1}{4\pi}\Sigma_{wr,g}(\bar{r})\phi_g(\bar{r})+\frac{1}{4\pi}\Sigma_{nr,g}(\bar{r})\Delta u_g \tag{2}$$

where

$$\begin{aligned}\int_g dE\;\Sigma_{t,g}(\bar{r},E)\psi_g(\bar{r},E,\hat{\Omega}) &= \frac{\int_g dE\;\Sigma_{t,g}(\bar{r},E)\psi_g(\bar{r},E,\hat{\Omega})}{\int_g dE\;\psi_g(\bar{r},E,\hat{\Omega})}\int_g dE\;\psi_g(\bar{r},E,\hat{\Omega})\\ &\approx \frac{\int_g dE\;\Sigma_{t,g}(\bar{r},E)\phi_g(\bar{r},E)}{\int_g dE\;\phi_g(\bar{r},E)}\int_g dE\;\psi_g(\bar{r},E,\hat{\Omega})\\ &= \Sigma_{t,g}(\bar{r})\psi_g(\bar{r},\hat{\Omega})\end{aligned}$$

In Eq. (2), $\Sigma_{t,g}(\bar{r})$ represents the self-shielded multigroup total cross section, defined as the CE total cross section collapsed with the CE scalar flux solution from Eq. (1). In addition, Δu_g is the lethargy width of group g. Rather than solve Eq. (1), ESSM introduces an equivalence-theory expression for each spatial region in the problem domain, i.e.,

$$(\Sigma_{t,g}(\bar{r})+\Sigma_{eq,g}(\bar{r}))\phi_g(\bar{r})=\Sigma_{wr,g}(\bar{r})\phi_g(\bar{r})+(\Sigma_{nr,g}(\bar{r})+\Sigma_{eq,g}(\bar{r}))\Delta u_g \tag{3}$$

Eq. (3) introduces the equivalence cross section, denoted $\Sigma_{eq,g}(\bar{r})$. By rearranging Eq. (3), and noting the relationship $\Sigma_{t,g}(\bar{r})=\Sigma_{a,g}(\bar{r})+\Sigma_{wr,g}(\bar{r})+\Sigma_{nr,g}(\bar{r})$, it can be shown [2] that

$$\Sigma_{eq,g}(\bar{r})=\frac{\Sigma_{a,g}(\bar{r})\phi_g(\bar{r})}{\Delta u_g-\phi_g(\bar{r})}-\Sigma_{nr,g}(\bar{r}) \tag{4}$$

where

$$\Sigma_{a,g}(\bar{r})\equiv\sum_i N_i(\bar{r})\sigma_{a,g,i}(\bar{r}) \tag{5}$$

$$\sigma_{a,g,i}(\bar{r})\equiv\sigma^{ref}_{a,g,i}\mathbf{F}_{a,g,i}\left(\sigma_{b,g,i}(\bar{r}),T(\bar{r})\right) \tag{6}$$

$$\sigma_{b,g,i}(\bar{r})\equiv\frac{1}{N(\bar{r})}\left(\Sigma_{nr,g}(\bar{r})+\Sigma_{eq,g}(\bar{r})\right)-\lambda_{g,i}\sigma_{p,i} \tag{7}$$

In Eq. (6), the nuclide-wise self-shielded multigroup absorption cross section is determined by Bondarenko interpolation, denoted $\mathbf{F}_{a,g,i}(\sigma,T)$. The interpolation is dependent on the nuclide-wise

background cross section $\sigma_{b,g,i}(\bar{r})$, and the spatial temperature distribution $T(\bar{r})$. $\sigma_{b,g,i}(\bar{r})$ is defined in Eq. (7), which is dependent on $\Sigma_{eq,g}(\bar{r})$. These equations show that the equivalence-theory expression introduces a nonlinear dependency in solving the multigroup slowing down equation (Eq. [2]), i.e., the cross sections in the multigroup slowing down equation depend on the multigroup slowing down flux solution. Therefore, an iterative procedure is employed to solve this equation, as follows:

1. Initialize $\Sigma_{eq,g}(\bar{r})$ to 0.0 or some *a priori* value.
2. Compute $\Sigma_{wr,g}(\bar{r})$ and $\Sigma_{nr,g}(\bar{r})$.
3. Compute $\Sigma_{a,g}(\bar{r})$ using Eq. (5), Eq. (6), and Eq. (7). Compute $\Sigma_{t,g}(\bar{r}) = \Sigma_{a,g}(\bar{r}) + \Sigma_{wr,g}(\bar{r}) + \Sigma_{nr,g}(\bar{r})$.
4. Solve the multigroup slowing down equation Eq. (2) for $\phi_g(\bar{r})$.
5. Compute new $\Sigma_{eq,g}(\bar{r})$ from $\phi_g(\bar{r})$ using Eq. (4). Eq. (4) can be solved for each spatial region in the problem or over each material region. The material region scalar flux is determined by flux-volume weighting of the spatial region scalar flux.[1]
6. Check for the convergence of $\Sigma_{eq,g}(\bar{r})$. If $\Sigma_{eq,g}(\bar{r})$ is not converged, go back to Step 3.

The iterative procedure is performed for each energy group, and each energy group calculation can be done in parallel. The description above is independent of the problem geometry (1-D, 2-D, or 3-D) and the underlying transport method. For Polaris, a 2-D method of characteristics (MoC) method is employed, and the energy groups are solved serially.[2]

The group-wise equivalence cross sections are stored in memory and used to prepare self-shielded multigroup cross sections for the k_{eff} calculation and the depletion calculation. The preparation of cross sections for these calculations is further described in Sect. 2.2.2.

2.2. Polaris k_{eff} Calculation

2.2.1. *Insilico MoC Solver*

The Polaris k_{eff} transport calculation uses the same 2-D MoC solver as the ESSM calculation. The MoC implementation in Polaris is similar to implementations in other lattice physics codes, with the following common features:

- Flat source approximation
- Uniformly spaced particle track lengths

[1] Polaris currently computes $\Sigma_{eq,g}(\bar{r})$ for each spatial region.
[2] Future versions of Polaris will enable energy parallelism.

- Exponential evaluation via table lookup
- Arbitrary scattering option or transport-corrected P_0 option
- Product quadrature sets
- Power iteration acceleration by the coarse mesh finite difference (CMFD) method.

The MoC solver was developed as part of the Insilico package of the Exnihilo code base (previously known as Denovo [4]). Polaris communicates with the Insilico MoC solver through a programming interface, with accessors to the flux, cross sections, source terms, and methods to construct the lattice geometry and to set solver options. The Exnihilo framework has been designed so that the 2-D MoC solver and the 3-D S_N solver use the same iterative methods (Krylov or stationary) and parallel energy decomposition methods. For the ESSM calculation, which requires 1-group fixed source calculations, Polaris can employ the GMRES or BiCGSTAB iterative method. In addition to CMFD acceleration for the k_{eff} calculation, Polaris can perform the power iteration using the GMRES or BiCGSTAB iterative methods to solve the fast-range within-group calculations and the thermal-range upscatter calculation.

The MoC particle track lengths are computed using the new ATLAS ray-tracing package in SCALE. ATLAS provides ray tracing for KENO-VI geometries and is currently used for model visualization and verification in addition to the MoC particle track length calculation.[3] The KENO-VI model of the lattice geometry is automatically generated by Insilico, based on the lattice geometry input provided through the programming interface. Currently, only square-pitched pressurized water reactor (PWR) geometries are supported through the Insilico-MoC programming interface.

2.2.2. *ESSM Coupling*

For k_{eff} calculation, the Insilico-MoC solver requires material-wise total, scatter, nu-fission, and chi macroscopic cross sections. For material m, these cross sections are denoted as $\Sigma_{t,g,m}$, $\Sigma_{l,m}^{g'\to g}$, $\nu\Sigma_{f,g,m}$, and $\chi_{g,m}$, respectively. The material cross sections are computed from the equivalence cross sections computed by the ESSM calculation. Given a cell-wise equivalence cross section of $\Sigma_{eq,g,c}$, the cell-wise nuclide background cross section for cell c and nuclide i is given by the following equation:

$$\sigma_{b,g,i,c} = \frac{1}{N_{i,m}}(\Sigma_{eq,g,c} + \Sigma_{g,c}^{BI}) - \sigma_{g,i,c}^{BI} \tag{8}$$

In Eq. (8), $N_{i,m}$ is the number density of nuclide i in material m and $\Sigma_{g,c}^{BI}$ represents the "homogeneous" component of the background cross section. Polaris supports the following options for computing $\Sigma_{g,c}^{BI}$:

[3] Atlas is intended for direct use in Monte Carlo simulations in future releases of SCALE.

$$\Sigma_{g,c}^{BI} \equiv \sum_i N_{i,m} \sigma_{g,i,c}^{BI} \tag{9}$$

$$\sigma_{g,i,c}^{BI} \equiv \begin{cases} \lambda_{g,i}\sigma_{p,i}, \\ \lambda_{g,i}\sigma_{p,i} + \sigma_{a,g,i,c}, \text{ or} \\ \lambda_{g,i}\sigma_{s,g,i,c} + \sigma_{a,g,i,c} \end{cases} \tag{10}$$

The last two options of Eq.(10) require Bondarenko iteration, as $\sigma_{g,i,c}^{BI}$ depends on the self-shielded microscopic cross sections $\sigma_{a,g,i,c}$ and/or $\sigma_{s,g,i,c}$. Given $\sigma_{b,g,i,c}$, self-shielded microscopic cross sections are determined by Bondarenko interpolation, i.e.,

$$\sigma_{x,g,i,c} \equiv \sigma_{x,g,i}^{ref} \mathbf{F}_{x,g,i}\left(\sigma_{b,g,i,c}, T_m\right) \tag{11}$$

where $\sigma_{x,g,i}^{ref}$ is the reference microscopic cross section for reaction x, T_m is the material temperature, and $\mathbf{F}_{x,g,i}(\sigma, T)$ represents the Bondarenko interpolation function. Polaris currently considers (n,γ), (n,s), and (n,f) reactions for self-shielding. The material-wise self-shielded microscopic cross sections are determined from $\sigma_{x,g,i,c}$ by flux-volume weighting, i.e.,

$$\sigma_{x,g,i,m} = \frac{\sum\limits_{c \in m} \sigma_{x,g,i,c}\phi_{g,c}V_c}{\phi_{g,m}V_m} \tag{12}$$

where $\phi_{g,c}$ is the cell-wise flux, V_c is the cell volume, $V_m \equiv \sum\limits_{c \in m} V_c$ is the material volume, and $\phi_{g,m} \equiv (1/V_m) \sum\limits_{c \in m} \phi_{g,c}V_c$ is the material-wise flux.

The material-wise macroscopic cross sections are computed from the values of $\sigma_{x,g,i,m}$. The equations for $\nu\Sigma_{f,g,m}$ and $\chi_{g,m}$ are as follows:

$$\nu\Sigma_{f,g,m} = \sum_i N_{i,m}\nu_{g,i}\sigma_{f,g,i,m} \tag{13}$$

$$\chi_{g,m} = \frac{\sum\limits_i N_{i,m} \sum\limits_{g'} \chi_i^{g' \to g} \nu_{g',i}\sigma_{f,g',i,m}\phi_{g',m}}{\sum\limits_g \nu\Sigma_{f,g,m}\phi_{g,m}} \tag{14}$$

where $\chi_i^{g' \to g}$ is the nuclide-wise chi from group g' to g. $\Sigma_{t,g,m}$ is computed as follows:

$$\Sigma_{t,g,m} = \Sigma_{t_0,g,m} + \sum_i N_{i,m} \sum_x \sigma_{x,g,i,m} \tag{15}$$

where $\Sigma_{t_0,g,m}$ accounts for cross-section reactions that are not self-shielded, i.e.,

$$\Sigma_{t_0,g,m} \equiv \sum_i N_{i,m}\sigma_{t_0,g,i} \tag{16}$$

$$\sigma_{t_0,g,i} \equiv \sigma_{(n,2n),i,g} + \sigma_{(n,n'),i,g} + \sigma_{(n,\alpha),i,g} + \cdots \tag{17}$$

In Eq. (17), the cross section $\sigma_{t_0,g,i}$ is dependent only on nuclide i and not material m and can be computed once for each nuclide in the cross-section library. The equation for $\Sigma_{l,m}^{g'\to g}$, where l denotes the scattering order, is given by the following:

$$\Sigma_{l,m}^{g'\to g} = \Sigma_{0,l,m}^{g'\to g} + \sum_i N_{i,m}\sigma_{s,g',i,m}\mathbf{G}_{s,l,i}^{g'\to g}(T_m) \tag{18}$$

where $\Sigma_{0,l,m}^{g'\to g}$ accounts for summation of all temperature-independent cross-section reactions that are not self-shielded and are scaled by the appropriate multiplicity, i.e.,

$$\Sigma_{0,l,m}^{g'\to g} \equiv \sum_i N_{i,m}\sigma_{0,l,i}^{g'\to g} \tag{19}$$

$$\sigma_{0,l,i}^{g'\to g} \equiv 2\sigma_{(n,2n),l,i}^{g'\to g} + 3\sigma_{(n,3n),l,i}^{g'\to g} + \sigma_{(n,n'),l,i}^{g'\to g} + \cdots \tag{20}$$

In Eq. (20), the cross section $\sigma_{0,l,i}^{g'\to g}$ is dependent only on nuclide i (not material m) and can be computed and stored for each nuclide in the cross-section library. In Eq. (18), $\mathbf{G}_{s,l,i}^{g'\to g}(T)$ represents a temperature interpolation function that returns the "normalized" 2-D scattering cross section at the given temperature. The term "normalized" implies that the appropriate self-shielded 2-D scattering cross section is produced from the output of $\mathbf{G}_{s,l,i}^{g'\to g}(T)$ multiplied by the self-shielded 1-D scattering cross section.

The k_{eff} calculation procedure is described as follows:

1. Initialize $\phi_{g,c}$ to 1.0 or some *a priori* value.
2. Compute and store $\Sigma_{t_0,g,m}$ and $\Sigma_{0,l,m}^{g'\to g}$ (Eq. [16], Eq. [17], Eq. [19], and Eq. [20]).
3. For each material m,
   (a) For each cell c in m, compute the nuclide-wise background cross section, i.e. $\sigma_{b,g,i,c}$, using Bondarenko iteration (Eq. [8], Eq. [9], and Eq. [10]).
   (b) For each cell c, compute nuclide-wise self-shielded microscopic cross sections, i.e., $\sigma_{x,g,i,c}$, for (n,γ), (n,s), and (n,f) using Bondarenko interpolation (Eq. [11]).

(c) Compute $\sigma_{x,g,i,m}$ using flux-volume weighting (Eq. [12]).

4. If material m is fissionable, compute material-wise nu-fission and chi by mixing the microscopic cross sections (Eq. [13] and Eq. [14]).
5. Compute the total cross section by mixing the self-shielded cross sections and adding the unshielded component $\Sigma_{t_0,g,m}$ from Step 2 (Eq. [15]).
6. Compute the scatter cross section by mixing the self-shielded scattering cross section and adding the unshielded component $\Sigma_{0,l,m}^{g' \to g}$ from Step 2 (Eq. [18]).
7. Solve for k_{eff} and $\phi_{g,c}$.
8. Check for the convergence of k_{eff} and $\phi_{g,c}$. If k_{eff} and $\phi_{g,c}$ are not converged, go back to Step 3.

2.3. Depletion, Input and Output, and Other Features

2.3.1. *Critical Bucking Search and Lattice Physics Edits*

After the k_{eff} transport calculation, Polaris performs a critical spectrum calculation for the homogenized fuel assembly. The critical spectrum calculation accounts for core leakage effects in an approximate manner for generating few-group homogenized cross sections and depletion reaction rates. The critical spectrum is optional and uses either the B_1 or P_1 approximation.

The cell-wise equivalence cross sections $\Sigma_{eq,g,c}$ and critical-spectrum-corrected flux are used in a similar procedure described in Sect. 2.2.2 for computing few-group homogenized cross-section and depletion reaction rates. Table I lists the different Polaris output edits available for downstream nodal code calculations.

2.3.2. *SCALE/ORIGEN Depletion Coupling*

Polaris is integrated with the SCALE/ORIGEN depletion and decay solver [5] for the depletion of material compositions. Polaris is coupled to the new object-oriented ORIGEN through a programming interface that provides the following functionality [6]:

- Accessors to set the initial nuclide concentration vector and transition matrix for a given material, along with various control options.
- A "solve" method in which Polaris invokes ORIGEN to deplete and/or decay the material over a series of timesteps.
- Accessors to retrieve the nuclide concentration vector over the series of timesteps.

Table I. Polaris lattice physics edits

Parameter	Description
k_∞	few-group k_∞
D_g	diffusion coefficient
$\Sigma_{a,g}$	absorption cross section
$\nu\Sigma_{f,g}$	nu-fission cross section
χ_g	chi fission spectrum
$\Sigma_{f,g}$	fission cross section
$\Sigma_s^{g'\rightarrow g}$	P_0 scattering matrix
$\kappa\Sigma_{f,g}$	energy released $\times$ fission cross section
Y_i	fission product yield for i equal I^{135}, Xe^{135}, and Pm^{149}
$\sigma_{a,g,i}$	microscopic absorbtion cross sections for i equal Xe^{135}, and Sm^{149}
ADF_g	assembly discontinuity factors (single assembly or reflector model)
CDF_g	corner discontinuity factors
PPF_g	pin power peaking factors
GFF_g	group-wise form factors
$1/v_g$	inverse velocity
$\beta_{eff,i}$	delayed neutron fraction for precursor group i
$\lambda_{eff,i}$	delayed neutron decay constant for precursor group i

- Accessors to set/retrieve nuclear data from the transition matrix. The cross sections in the ORIGEN transition matrix are updated by collapsing the material-wise microscopic cross sections with the material-wise critical-spectrum-corrected flux distribution.

Polaris currently implements a predictor-only substep depletion algorithm. In this algorithm, Polaris computes the number of timesteps and the size of each timestep based on user-provided burnups (GWD/t) and the specific power (MW/t) for each burnup step. Polaris also computes a set of internal substeps per timestep, which are used for the ORIGEN depletion calculation. The depletion algorithm proceeds as follows:

1. At the beginning of each timestep:
   (a) Perform the ESSM calculation.
   (b) Perform the k_{eff} calculation.
   (c) Perform the critical spectrum calculation.
2. Update the ORIGEN transition matrix for each depletion material by energy-group collapsing the material-wise microscopic cross sections with the material-wise flux.
3. For each substep:
   (a) Compute the normalized material-wise flux based on the beginning-of-*substep* material-wise nuclide concentrations, beginning-of-*timestep* material-wise flux distribution, and beginning-of-*timestep* cross sections.

(b) Deplete each material with ORIGEN for one substep.

(c) Repeat for each substep in the timestep.

4. Repeat for each timestep.

2.3.3. *Data Libraries and Input Format*

Polaris currently uses either a 252-group or a 56-group library, both generated with the AMPX code system [7] from ENDF/B-VII-based data evaluations. The library contains cross sections, IR parameters, and full-range Bondarenko factors for 422 nuclides. Bondarenko factors for ^{235}U, ^{238}U, ^{239}Pu, ^{240}Pu, and ^{241}Pu were generated based on heterogeneous equivalence theory, a procedure that ensures the ESSM calculation reproduces the self-shielded cross sections computed from a series of reference 2-D MoC CE unit cell calculations. The set of unit cell configurations was selected to span the range of self-shielding for these isotopes for LWR analysis.

Polaris employs an easy-to-use input file format similar to industry lattice physics codes. An LWR assembly model can be generated with approximately 50 lines of input compared with the approximately 1000 lines of input for an equivalent TRITON model.

3. BENCHMARK RESULTS

3.1. VERA UO_2 Benchmarks

The Virtual Environment for Reactor Applications (VERA) benchmark progression problems have been established to measure the progress and assess the accuracy of emerging LWR simulation capabilities within the Consortium for Advanced Simulation of Light Water Reactors (CASL) [8]. The benchmarks are derived from actual fuel and plant data from the initial core loading of Watts Bar Unit 1, a PWR with Westinghouse 17×17 fuel assemblies. Polaris calculations were performed for the first and second problem sets of the VERA benchmark progression problems, which contain 5 pin cell benchmarks and 17 lattice benchmarks, respectively.

The full description for the VERA benchmark problems is provided in Ref. [8]. The problems have been developed for fresh UO_2 fuel (3.1% ^{235}U enrichment) and at the hot-zero-power (HZP) beginning-of-cycle critical boron condition of ˜1300 ppm boron. A brief description for each of the benchmark problems modeled in this work is provided in Table II. Unless otherwise stated in Table II, all material temperatures are modeled at 600°K, and the coolant density is modeled at 0.743 g/cm^3.

For all VERA benchmark calculations, a Tabuchi-Yamamoto [9] product quadrature set was used with three polar angles per octant, 20 azimuthal angles per octant, and a ray spacing of 0.03 cm. For the integrable fuel burnable absorber (IFBA) –loaded cases (2L, 2M, and 2N), 0.003 cm ray spacing was selected to appropriately model the thermal flux depression in the IFBA coating. An

approach to reduce the ray spacing for IFBA problems, via homogenization or an alternative approach, remains under investigation.

Table II. VERA benchmark description

ID	Pin Cell Description
1A	565°K
1B	0.661 g/cm^3
1C	0.661 g/cm^3, 900°K fuel
1D	0.661 g/cm^3, 1200°K fuel
1E	0.001 cm IFBA[a](ZrB_2)
ID	**Lattice Description**
2A	565°K
2B	0.661 g/cm^3
2C	0.661 g/cm^3, 900°K fuel
2D	0.661 g/cm^3, 1200°K fuel
2E	12 Pyrex poison rods
2F	24 Pyrex poison rods
2G	24 Ag-In-Cd control rods
2H	24 B_4C control rods
2I	Instrument thimble
2J	Instrument thimble + 24 Pyrex
2K	Radially-zoned enrichment + 24 Pyrex
2L	80 IFBA
2M	128 IFBA
2N	104 IFBA + 20 WABA[b]
2O	12 Gd_2O_3-integral burnable absorber rods
2P	24 Gd_2O_3-integral burnable absorber rods
2Q	Spacer grid[c]

[a] Integral fuel burnable absorber.
[b] Wet annular burnable absorber.
[c] Polaris cannot model spacer grids explicitly.

Table III shows the Polaris k_{eff} values for the five pin cell benchmarks, compared with reference CE KENO-VI results provided in Ref. [8]. Polaris exhibits a slight temperature bias in cases 1B through 1D, in which the reactivity difference decreases as the fuel temperature increases. Investigations have shown that this bias can be minimized with an improved treatment for the temperature dependence of the removal cross section.[4] The VERA pin cell benchmarks were also modeled with Polaris and as part of the SCALE/Sampler sequence to quantify the impact of cross-section uncertainty on pin-cell k_{eff}. The final column in Table III provides the uncertainty in k_{eff} as computed by SCALE/Sampler. The relative standard deviation in k_{eff} due to uncertainty in the cross sections is approximately 0.5% (or 500×10^5).

[4] In future development, an additional Bondarenko factor for the removal cross section will be introduced to the multigroup library, and the scattering matrices will be renormalized to account for the self-shielding of the removal cross section.

Table III. VERA pin cell benchmark Polaris results

ID	CE-KENO-VI k_{eff} (SD[a])	Polaris k_{eff}	$\Delta\rho$ (pcm)	Sampler-Polaris XS (RSD[b])
1A	1.18782 (7)	1.18631	−107	491
1B	1.18294 (7)	1.18143	−108	508
1C	1.17239 (8)	1.16999	−174	512
1D	1.16315 (7)	1.16015	−222	516
1E	0.77237 (8)	0.77101	−228	562

[a] Standard deviation from CE-KENO-VI ($\times 10^5$).
[b] Relative standard deviation from Sampler-Polaris ($\times 10^5$).

Table IV shows the Polaris calculation result for 16 VERA lattice benchmarks, compared with reference CE KENO-VI results provided in Ref. [8]. Both reactivity differences and normalized pin-wise fission rate differences are provided. The CE KENO-VI uncertainties are approximately 2×10^5 for k_{eff} and less than 0.06% for normalized pin fission rates. Polaris exhibits a slight temperature bias in cases 2B through 2D, in which the reactivity difference decreases as the fuel temperature increases. For the the pin and lattice benchmarks, the results demonstrate that Polaris provides acceptable predictions for HZP beginning-of-life PWR pin and lattice calculations.

Figure 1 shows the pin power distribution for VERA lattice 2B, compared with reference CE KENO-VI results provided in Ref. [8]. The lattice map on the right of 1 shows the absolute difference between the calculations in units of percent. The Polaris pin powers are in good agreement with the reference solution. The RMS difference is 0.08% and the max difference is 0.19%. VERA lattice 2B was also simulated with the SCALE/Sampler sequence, and the pin power uncertainties are presented in Figure 1. The pin power uncertainties due to cross-section uncertainties are ˜0.008% absolute standard deviation, and the uncertainty in k_{eff} is 1.18243 ± 0.00490.

4. CONCLUSION

Polaris is a new 2-D PWR lattice physics capability for the SCALE code system. In this paper, the implementation of the Polaris calculation methods is summarized and calculation results are provided for the CASL VERA computational benchmarks. The results demonstrate that Polaris provides acceptable predictions for HZP beginning-of-life PWR pin and lattice calculations.

Polaris can also be used for lattice physics uncertainty quantification as part of the SCALE/Sampler sequence. Uncertainties in lattice k_{eff} and pin powers were demonstrated for the CASL VERA computational benchmarks.

Several development efforts are ongoing before the official release of Polaris in SCALE 6.2. These efforts include addressing the bias in k_{eff} as a function of fuel temperature, the implementation of branch calculations and time-dependent changes to system parameters, and further benchmarking

Table IV. VERA pin cell benchmark results

ID	CE KENO-VI k_{eff} (SD[a])	Polaris k_{eff}	$\Delta\rho$ (pcm)	Pin power, %[b] (RMS)	Pin power, % (max)
2A	1.18273 (2)	1.18252	−15	0.07 %	0.21 %
2B	1.18403 (2)	1.18243	−114	0.08 %	0.19 %
2C	1.17443 (2)	1.17201	−176	0.08 %	0.15 %
2D	1.16614 (2)	1.16301	−231	0.08 %	0.17 %
2E	1.07044 (3)	1.06939	−92	0.07 %	0.18 %
2F	0.97690 (3)	0.97620	−73	0.09 %	0.21 %
2G	0.84924 (2)	0.84881	−59	0.19 %	0.37 %
2H	0.78975 (2)	0.79102	203	0.17 %	0.36 %
2I	1.18056 (2)	1.17888	−121	0.08 %	0.20 %
2J	0.97610 (2)	0.97547	−66	0.09 %	0.21 %
2K	1.02100 (2)	1.02025	−72	0.10 %	0.26 %
2L	1.01954 (2)	1.01781	−167	0.11 %	0.23 %
2M	0.93946 (3)	0.93775	−194	0.12 %	0.25 %
2N	0.87043 (3)	0.86910	−176	0.12 %	0.27 %
2O	1.04837 (2)	1.04744	−85	0.11 %	0.28 %
2P	0.92800 (3)	0.92769	−36	0.14 %	0.32 %

[a] Standard deviation from CE KENO-VI ($\times 10^5$).
[b] Pin powers are actually normalized fission rates.

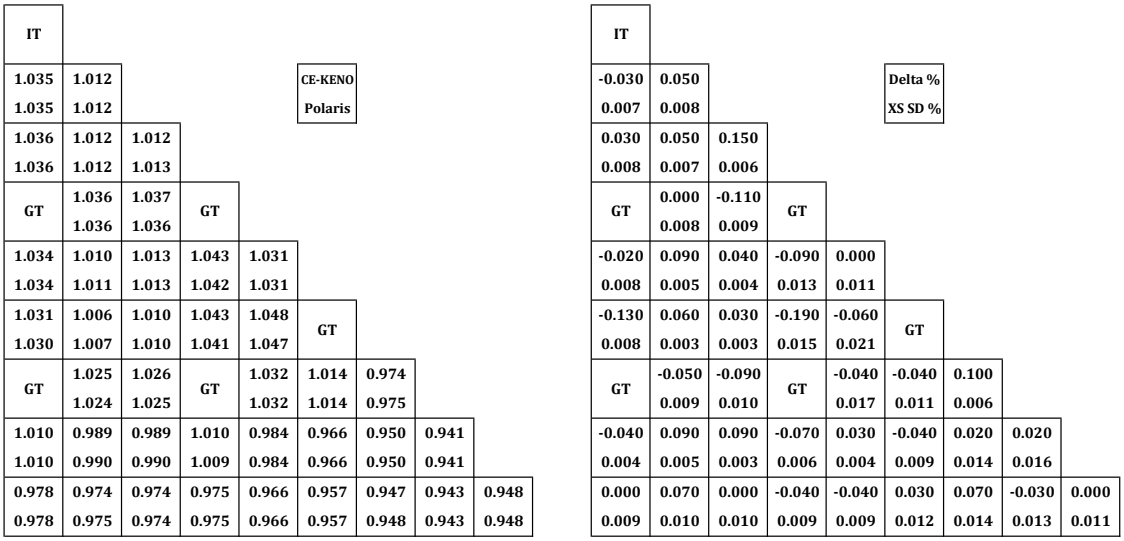

Figure 1. Pin power comparison for VERA lattice 2B.

calculations focused on depletion calculations. Longer-term efforts include implementing a gamma transport capability, a multi-bundle analysis capability, support for boiling water reactor, CANDU, and VVER lattice geometries, and a user-defined general-geometry capability.

ACKNOWLEDGMENTS

The authors would like to thank the US Nuclear Regulatory Commission for the development of Polaris.

REFERENCES

[1] *SCALE: A Comprehensive Modeling and Simulation Suite for Nuclear Safety Analysis and Design*. Available from Radiation Safety Information Computational Center at Oak Ridge National Laboratory as CCC-785 (2011).

[2] Mark L. Williams and Kang Seog Kim. "The Embedded Self-Shielding Method." In: *PHYSOR 2012*. Knoxville, Tennessee, USA (2012).

[3] M. L. Williams *et al.* "A Statistical Sampling Method for Uncertainty Analysis with SCALE and XSUSA." *Nuclear Technology*, **183(3)**: pp. 515–526 (2013).

[4] T. M. Evans *et al.* "Denovo: A New Three-Dimensional Parallel Discrete Ordinates Code in SCALE." *Nuclear Technology*, **171(2)**: pp. 171–200 (2010).

[5] I. C. Gauld *et al.* "Isotopic Depletion and Decay Methods and Analysis Capabilities in SCALE." *Nuclear Technology*, **174(2)**: pp. 169–195 (2011).

[6] S. Skutnik *et al.* "Development of an Object-oriented ORIGEN for Advanced Nuclear Fuel Modeling Applications." In: Proc. Int. Conf. *Mathematics and Computational Methods Applied to Nuclear Science and Engineering (M&C 2013)*. American Nuclear Society, Sun Valley, Idaho, USA, May 5–9, 2013 (2013).

[7] M. E. Dunn and M. N. Greene. "AMPX-2000: A Cross-Section Processing System for Generating Nuclear Data for Criticality Safety Applications." *Transactions of American Nuclear Society*, **86**: pp. 118–119 (2002).

[8] A. T. Godfrey. "VERA Core Physics Benchmark Progression Problem Specifications." URL http://www.casl.gov/docs/VERA_Benchmarks_1-5_r2_disclaimer.pdf. CASL Technical Report, CASL-U-2012-0131-002 (2013).

[9] A. Yamamoto *et al.* "Derivation of Optimum Polar Angle Quadrature Set for the Method of Characteristics Based on Approximation Error for the Bickley Function." *Journal of Nuclear Science and Technology*, **44(2)**: pp. 129–136 (2007).